

# Energy

A Bidirectional LLC Converter using Common Mode and Differential Mode Current Injection.....	45
Electro-Chemo-Mechanical Studies of Perovskite-structured Mixed Ionic-electronic Conducting $\text{SrSn}_{1-x}\text{Fe}_x\text{O}_{3-x/2+\delta}$ .....	46
High Capacity CMOS-compatible Thin Film Batteries on Flexible Substrates.....	47
Kinetic Study of Lithiation-induced Crystallization in Amorphous Germanium Anodes in Thin Film Batteries .....	48
Mechanisms of Li Storage in $\text{RuO}_2$ Electrodes for Thin Film Batteries .....	49
Crystal Engineering of Mixed Cation Perovskite for Fabrication of Highly Efficient Solar Cells.....	50
Buckled MEMS Beams for Energy Harvesting from Low-frequency Vibrations .....	51
A Robust Electromagnetic MEMS Vibration Energy Harvester .....	52
Foulant-agnostic Coatings for Extreme Environments.....	53
All-solid-state Glucose Fuel Cell for Energy Harvesting in the Human Body.....	54



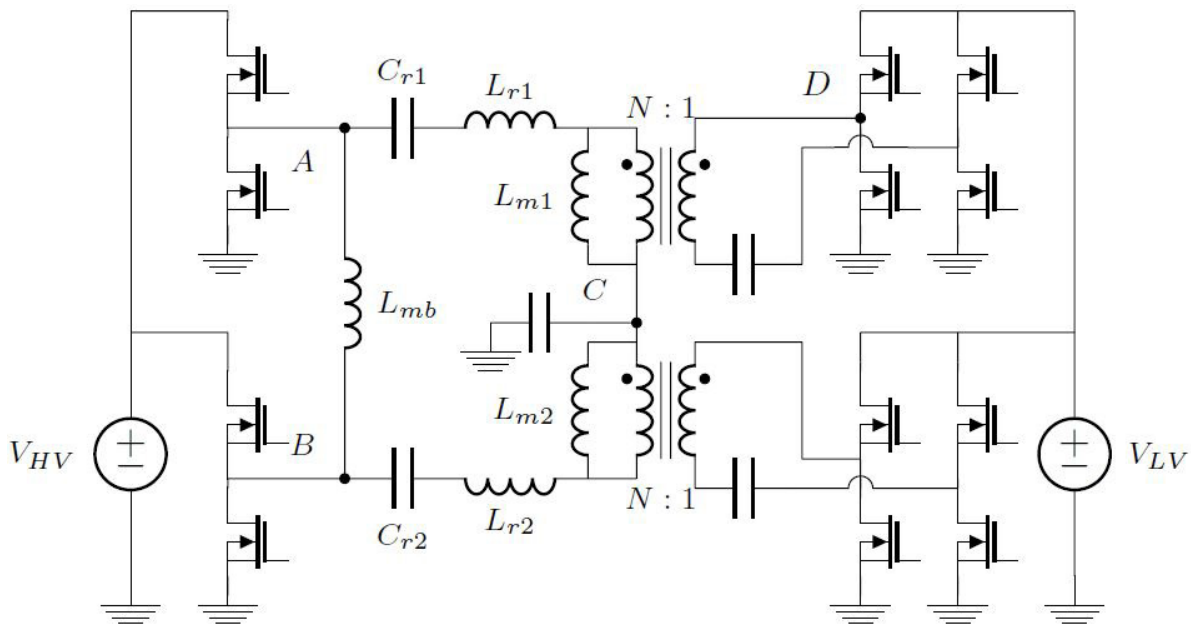
# A Bidirectional LLC Converter using Common Mode and Differential Mode Current Injection

J. D. Boles, J. A. Santiago-Gonzalez, D. M. Otten, D. J. Perreault  
Sponsorship: Bosch, NSF GRFP

Power converters are ubiquitous in today's world of electronics, and the push for higher-power-density converters has opened new realms of applications for them. One popular converter topology for high-performance, high-power-density converters is the LLC resonant converter, which relies on the frequency-dependent gain of an LLC network for voltage conversion. This LLC network consists of a capacitor, inductor, and transformer in series, with the transformer's magnetizing inductance serving as the LLC's second inductance. This LLC network's gain characteristic is advantageous because it allows the converter to achieve a wide range of input/output voltage gain with only a narrow range of switching frequencies. However, with a traditional LLC converter, this valuable gain characteristic is present for power conversion only in the forward direction. This trait is inopportune for bidirectional converters.

In this work, we have demonstrated a converter topology that achieves the LLC gain characteristic

during both forward and backward operation. This topology splits the traditional LLC topology into two equal halves, as Figure 1 illustrates. Then, we add an auxiliary inductor  $L_{mb}$  between the two inverter switch nodes to serve the magnetizing inductance role during reverse operation. Both halves are driven identically in parallel (the voltages at points A and B are always equal) for forward operation, resulting in common-mode current injection into the LLC resonant tank and no current through the auxiliary inductor. During reverse operation, the two halves are driven 180 degrees apart, resulting in differential-mode current injection that passes through the auxiliary inductor. As a result, the resonant tank exhibits a gain characteristic resembling that of an LLC network in both directions. This topology brings the high-performance of LLC resonant converters to a variety of new applications requiring bidirectional power flow, such as consumer electronics, electric vehicles, and grid energy storage.



▲ Figure 1: Proposed bidirectional LLC converter topology. During forward operation, two halves operate in parallel, and  $L_{mb}$  is unused. During reverse operation, current circulation through  $L_{mb}$  helps recreate the advantageous LLC gain curve.

## FURTHER READING

- J. D. Boles, J. A. Santiago-Gonzalez, D. M. Otten, and D. J. Perreault, "A Bidirectional LLC Converter Enabled by Common Mode and Differential Mode Current Injection," *Proc. IEEE Energy Conversion Congress and Exposition (ECCE)*, Sep. 2019.

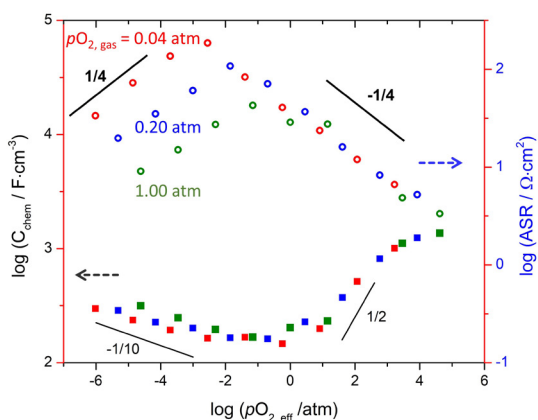
# Electro-Chemo-Mechanical Studies of Perovskite-structured Mixed Ionic-electronic Conducting $\text{SrSn}_{1-x}\text{Fe}_x\text{O}_{3-x/2+\delta}$

C.-S. Kim, S. R. Bishop, N. H. Perry, H. L. Tuller  
Sponsorship: Skolkovo Foundation

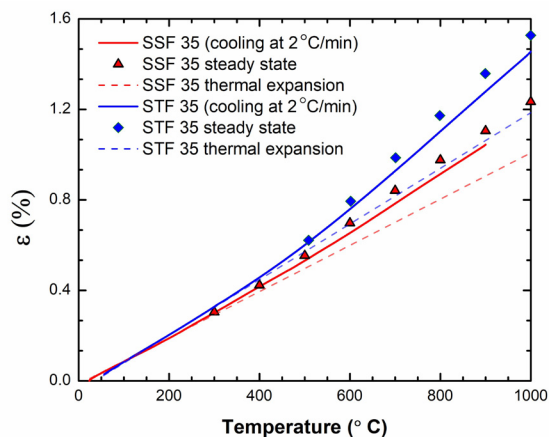
Solid oxide fuel cells (SOFCs) convert chemical energy directly to electricity and thus have high potential conversion efficiency. Thermo-mechanical stability and high cathode surface reaction kinetics are two major criteria for good SOFC cathodes. In this work, we extend previous studies on the promising mixed ionic and electronic conducting perovskite-structured  $\text{SrTi}_{1-x}\text{Fe}_x\text{O}_{3-x/2+\delta}$  (STF) materials system whose exchange kinetics were correlated with the minority electron charge density by replacing Ti with Sn, due to its distinct band structure and higher electron mobility.

Oxygen nonstoichiometry and the defect chemistry of the  $\text{SrSn}_{1-x}\text{Fe}_x\text{O}_{3-x/2+\delta}$  (SSF) system were examined by thermogravimetry as a function of oxygen partial pressure in the temperature range of 973-1273 K. Marginally higher reducibility was observed compared to corresponding compositions in the STF system. The bulk electrical conductivity was measured in parallel to examine how changes in defect chemistry and electronic band structure, associated with the

substitution of Ti by Sn, impact carrier density and ultimately electrode performance. Bulk chemical expansion was measured by dilatometry as a function of oxygen partial pressure while surface kinetics were examined using AC impedance spectroscopy. The electrochemical properties of SSF were found not to differ significantly from the corresponding composition in STF. Though slightly shifted by the larger size of Sn, the defect equilibria and the cathode area specific resistance differed only in a limited way from that in STF. This small difference was attributed to properties being largely dominated by Fe and not by the substitution of Ti with Sn. However, due to asymmetry in the crystal structure caused by the larger size of Sn, both thermal and chemical expansion coefficients of SSF35 were found to be around 20% and 10% lower, respectively, than those of STF35, thus making SSF35 much more chemo-mechanically stable in SOFC operating conditions.



▲ Figure 1: Oxygen nonstoichiometry  $\delta$  as a function of  $p_{\text{O}_2}$  and temperature for SSF35.



▲ Figure 2: Measured strains (solid lines), thermal expansions extended from low-temperature regimes (dashed lines) and steady-state strains (points) of SSF35 (red) and STF35 (blue).

## FURTHER READING

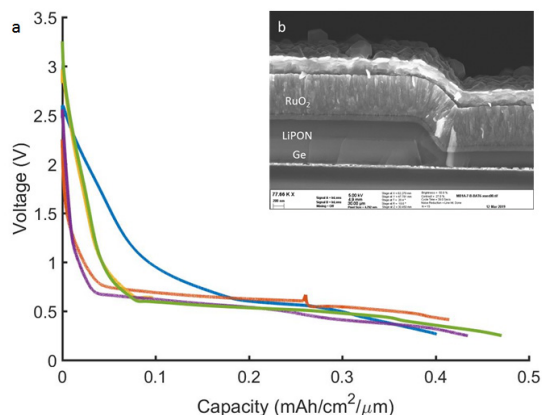
- C.-S. Kim, S. R. Bishop, and H. L. Tuller, "Electro-chemo-mechanical Studies of Perovskite-structured Mixed Ionic-electronic Conducting  $\text{SrSn}_{1-x}\text{Fe}_x\text{O}_{3-x/2+\delta}$  Part II: Electrical Conductivity and Cathode Performance," *J. Electroceram.*, vol. 40, pp. 57-64, 2018.
- C.-S. Kim, N. H. Perry, S. R. Bishop, and H. L. Tuller, "Electro-chemo-mechanical Studies of Perovskite-structured Mixed Ionic-electronic Conducting  $\text{SrSn}_{1-x}\text{Fe}_x\text{O}_{3-x/2+\delta}$  Part III: Thermal and Chemical Expansion," *J. Electroceram.*, 2018.
- C.-S. Kim, S. R. Bishop, and H. L. Tuller, "Electro-chemo-mechanical Studies of Perovskite-structured Mixed Ionic-electronic Conducting  $\text{SrSn}_{1-x}\text{Fe}_x\text{O}_{3-x/2+\delta}$  Part I: Defect Chemistry," *J. Electroceram.*, vol. 38, pp. 74-80, 2017.

# High Capacity CMOS-compatible Thin Film Batteries on Flexible Substrates

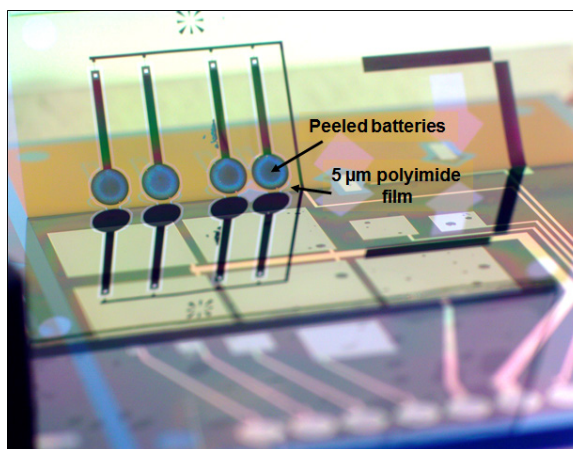
M. J. Chon, A. Weathers, M. Polking, J. Kedzierski, D. Nezich, H. Chea, L. Racz, C. V. Thompson  
Sponsorship: Lincoln Laboratories

The miniaturization of sensors through advancements in low-powered MEMS devices in integrated circuits has opened up new opportunities for thin film microbatteries. However, many of the available thin film battery materials require high-temperature processes that necessitate additional packaging materials, which reduce the overall energy density of these batteries. Previous research with collaborators in Singapore demonstrated an all-solid-state materials system with high volumetric capacity that exclusively utilizes CMOS-compatible (i.e., room temperature) processes. This process allows integration of these batteries with CMOS circuits as distributed power supplies or for integrated autonomous microsystems. Additionally, the ability to deposit all components of the battery at room temperature makes it possible to fabricate these batteries on thin, flexible substrates that can be densely stacked to achieve energy densities comparable to bulk batteries, which has been the focus of this project.

We have successfully demonstrated a full thin film microbattery using germanium (Ge) and ruthenium dioxide ( $\text{RuO}_2$ ) as anode and cathode materials, respectively, with lithium phosphorous oxynitride (LiPON) as the solid-state electrolyte (Figure 1b). Although  $\text{RuO}_2$  has traditionally been used as an anode material, it has significantly higher volumetric capacity than typical cathode materials and sufficiently high electrochemical potential versus Ge to provide an output voltage of about 0.5V at a capacity of about  $40 \text{ Ah/cm}^3$  (Figure 1a). These materials are deposited onto a thin ( $\sim 5 \mu\text{m}$ ), flexible polyimide substrate with integrated interconnects and peeled off the handle substrate (Figure 2). These battery films can be stacked for higher power and energy densities and folded to fit any volume.



▲ Figure 1: (a) Voltage profile of a full battery during discharge. (b) Scanning electron microscope image showing the components of the solid-state microbattery. The LiPON and  $\text{RuO}_2$  layers were sputter deposited, allowing them to fully conform over the edge of the Ge anode.



▲ Figure 2: Peeling of batteries deposited on a polyimide membrane off the silicon handle substrate.

## FURTHER READING

- D. Perego, J. S. T. Heng, X. Wang, Y. Shao-Horn, and C. V. Thompson, "High-performance Polycrystalline  $\text{RuO}_x$  Cathodes for Thin Film Li-ion Batteries," *Electrochimica Acta*, vol. 283, pp. 228-233, Sep. 2018.

# Kinetic Study of Lithiation-induced Crystallization in Amorphous Germanium Anodes in Thin Film Batteries

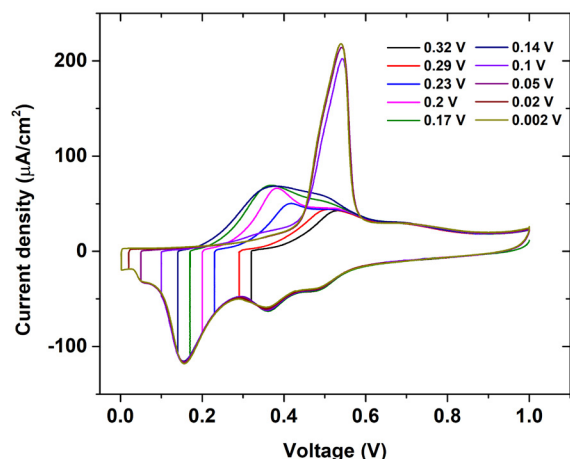
J. Miao, B. Wang, C. V. Thompson

Sponsorship: Singapore-MIT Alliance for Research and Technology

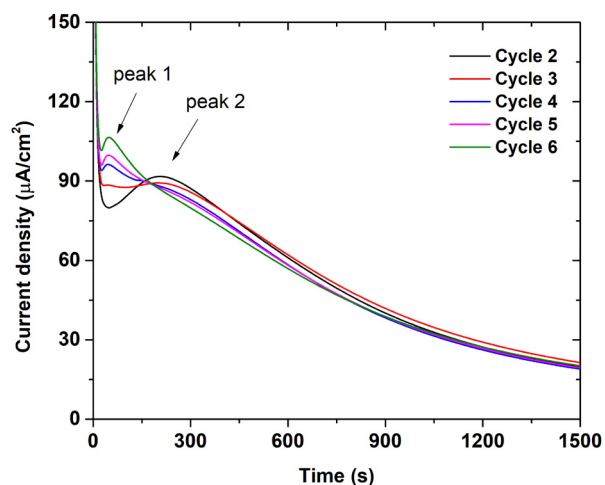
Germanium (Ge) is one of the most promising anode materials for complementary metal-oxide semiconductor (CMOS)-compatible lithium-ion microbatteries. An intercalation or allowing anode is needed to avoid the presence of metallic Li for this application. Ge has a volumetric capacity of 7366 mAh/cm<sup>3</sup>, which is ten times as large as the graphite anodes used in commercial bulk batteries. When Ge is discharged below a threshold voltage, a crystalline phase Li<sub>15</sub>Ge<sub>4</sub> forms. This phase is expected to affect the performance of Ge anodes. The degree of crystallinity is hugely affected by the cutoff voltage during lithiation (Figure 1), as well as other factors including cycle number and initial film thickness. In addition to structural analyses and cyclic voltammetry techniques, we have developed a potentiostatic technique to study the kinetics of crystallization at low

voltage in amorphous Ge anodes.

We found double peaks in the current vs. time curves under specific potentiostatic test conditions (Figure 2). The existence of double peaks indicates that two phase transitions occur under the given conditions. The appearance of peak 1 in Figure 2 exhibits clear correlations with the applied voltage, cycle number, and initial film thickness, which all indicate the formation of the c-Li<sub>15</sub>Ge<sub>4</sub> phase. Combining kinetic studies with previously reported spectroscopic studies, we can attribute peak 1 to the amorphous-to-crystalline transition, while peak 2 corresponds to an amorphous-to-amorphous transition. The extent to which the crystalline phase forms has a dramatic effect on the delithiation behavior (Figure 1).



▲ Figure 1: Current-voltage curves (cyclic voltammograms) for Ge thin films lithiated to different cutoff voltages and held for 8 hours. Intensity of sharp peak at 0.55 V indicates amount of c-Li<sub>15</sub>Ge<sub>4</sub> formed at end of lithiation.



▲ Figure 2: Current vs. time curves in different cycles for potentiostatic tests at 200 mV in LiPON-coated germanium thin film (200-nm thick).

## FURTHER READING

- A. Al-Obeidi, D. Kramer, R. Mönig, and C. V. Thompson, C. V. "Mechanical Stresses and Crystallization of Lithium Phosphorous Oxynitride-coated Germanium Electrodes during Lithiation and Delithiation," *J. of Power Sources*, vol. 306, pp. 817-825, 2016.
- A. Al-Obeidi, D. Kramer, C. V. Thompson, and R. Mönig, "Mechanical Stresses and Morphology Evolution in Germanium Thin Film Electrodes during Lithiation and Delithiation," *J. of Power Sources*, vol. 297, pp. 472-480, 2015.

# Mechanisms of Li Storage in RuO<sub>2</sub> Electrodes for Thin Film Batteries

L. Xu, C. V. Thompson

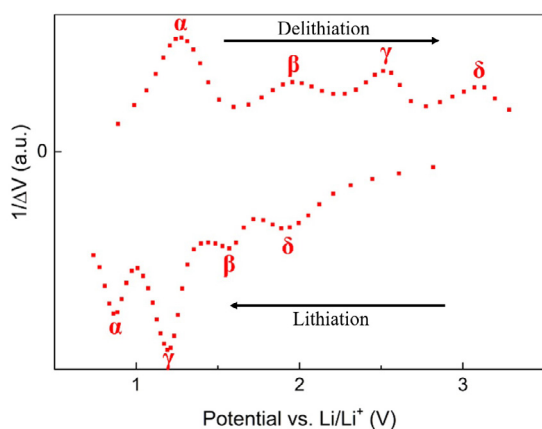
Sponsorship: Skotech Center for Electrochemical Energy Storage

It has been demonstrated that RuO<sub>2</sub> films can serve as high-performance electrodes for thin film lithium-ion batteries due to their large volumetric charge capacity, excellent cyclability, and rate capability. Unlike other electrode materials, RuO<sub>2</sub> films also do not require high-temperature processing, making them suitable for integration with low-power CMOS circuits and fabrication on flexible membranes. However, lithiation and delithiation mechanisms for RuO<sub>2</sub> are poorly understood, and an improved understanding is required for optimization of battery performance and yield.

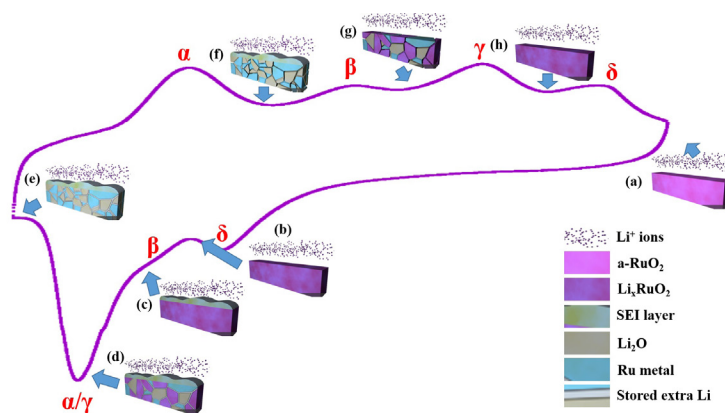
Lithium is stored in RuO<sub>2</sub> films through a complex sequence of phase transformations. We have carried out detailed electrochemical studies coupled with the physical characterization of sputtered RuO<sub>2</sub> thin films. The sequence of phase transformations during lithiation and delithiation was electrochemically characterized using galvanostatic intermittent titration technique (GITT) and cyclic voltammetry (CV) measurements (Figure 1). These characterizations

were correlated with ex-situ selected area electron diffraction (SAED), X-ray photoelectron spectroscopy (XPS), Raman spectroscopy, optical microscopy (OM), scanning electron microscopy (SEM), energy-dispersive X-ray spectroscopy (EDS), and in-situ electrochemical impedance spectroscopy (EIS) results. This allows identification of phase transformations  $\alpha$ ,  $\beta$ ,  $\gamma$ , and  $\delta$  as reactions of Li storing between the grain boundaries between nanosized grains, formation of a reversible SEI layer, main conversion reaction, and formation of alloy Li<sub>x</sub>RuO<sub>2</sub>, respectively, as Figure 2 shows. Current studies are focused on application of these insights to optimization of the performance of RuO<sub>2</sub> electrodes in full thin film batteries.

The methodology developed in this study can also be applied to other candidate thin film electrode materials. In addition, lessons from studying thin films can be applied to more complex powder-based electrodes used in bulk batteries.



◀ Figure 1:  $1/\Delta V$  vs. voltage curve extracted from GITT tests of a RuO<sub>2</sub>/LiPF<sub>6</sub>/Li cell. The peaks with the same label are from one reaction and its corresponding reverse reaction.



▲ Figure 2: Proposed sequence of phase transformations during lithiation and delithiation of RuO<sub>2</sub> films.

# Crystal Engineering of Mixed Cation Perovskite for Fabrication of Highly Efficient Solar Cells

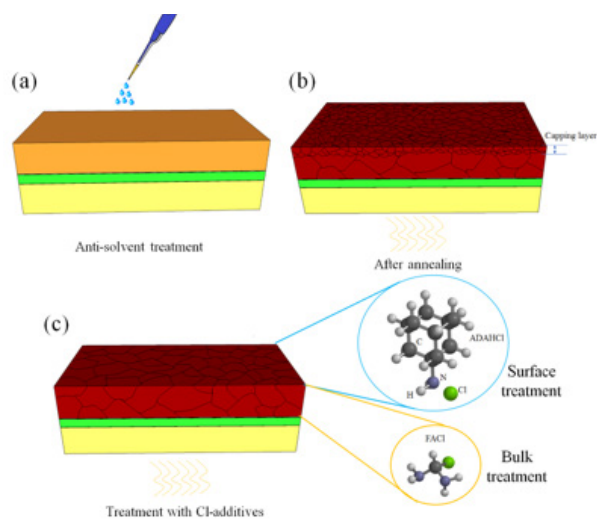
M. M. Tavakoli, J. Kong  
Sponsorship: ENI S.p.A

Inorganic-organic perovskite solar cells (PSCs) have caught tremendous interest from many research groups in the field of photovoltaic devices due to their low cost, ease of fabrication, and excellent optical and electrical properties, which resulted in a record certified personal consumption expenditure (PCE) of 23.3%. The presence of surface and grain boundary defects in organic-inorganic halide perovskite films is detrimental to both the performance and operational stability of PSCs. Here, we study the effect of chloride (Cl) additives on the bulk and surface defects of mixed-cation and halide PSCs. We found that using an anti-solvent technique divides the perovskite film into two separate layers, i.e., a bottom layer with large grains and a thin capping layer with small grains.

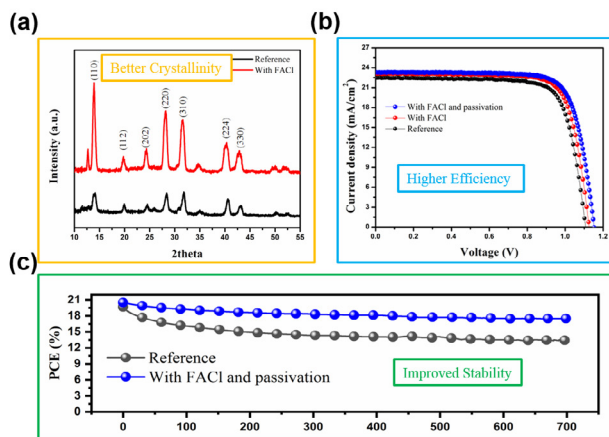
Moreover, we demonstrate that the addition of formamidinium chloride (FACl) into the precursor solution removes the small grain perovskite capping layer and suppresses the formation of bulk and surface defects (Figure 1). This modification by FACl provides the perovskite film with remarkably improved orientation, crystallinity, and large grain size up to over 1  $\mu\text{m}$  (Figure 2a). Time-resolved photoluminescence measurements show longer lifetimes for perovskite

films modified by FACl and subsequently passivated by 1-adamantylamine hydrochloride (ADAHCl) than for the reference sample. Based on these treatments, we improve the quality of perovskite film and increase the power conversion efficiency (PCE) from 19.43% for a reference sample to 21.2% for the modified device by Cl additives. This efficiency is among the highest reported values for a planar perovskite solar cell. This PCE enhancement is mostly due to the improvement of open circuit voltage ( $V_{oc}$ ) from 1110 mV to 1152 mV (Figure 2b).

Moreover, the device modified by Cl additives shows a lower hysteresis effect than the reference sample. Importantly, the molecular engineering created by applying Cl additives greatly enhances the stability of the PSCs, which show only 5% degradation after aging for 90 days, which is higher than the 16% PCE loss of the reference device (Figure 2c). Additionally, we found that the modified device with Cl additives shows a smaller ideality factor of 1.8 than 2.1 for the reference device, due to the lower recombination. Our proposed approach opens up a new direction for the commercialization of efficient and stable solar cell devices.



▲ Figure 1. Schematic depiction of perovskite films fabricated by the anti-solvent method on  $\text{SnO}_2$ -coated FTO glass before (a) and after (b) annealing and after treatment with Cl additives (c).



▲ Figure 2. (a) X-ray diffraction patterns of perovskite films for reference sample and perovskite with the FACl additive. (b) Current density-voltage curve and (c) operational stability measurement under continuous illumination for the corresponding PSCs.

## FURTHER READING

- M. M. Tavakoli, P. Yadav, D. Prochowicz, M. Sponseller, A. Osherov, V. Bulović, and J. Kong, "Controllable Perovskite Crystallization via Antisolvent Technique using Chloride Additives for Highly Efficient Planar Perovskite Solar Cells," *Adv. Energy Mater.* 2019, 9, 1803587.

# Buckled MEMS Beams for Energy Harvesting from Low-frequency Vibrations

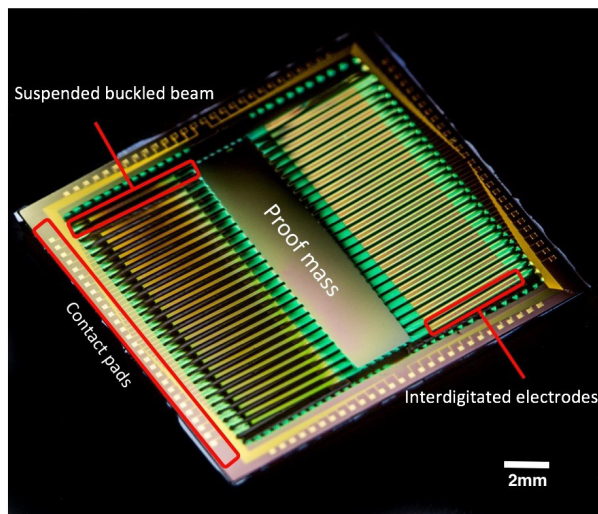
R. Xu, H. Akay, S-G. Kim

Sponsorship: MIT-SUTD International Design Center

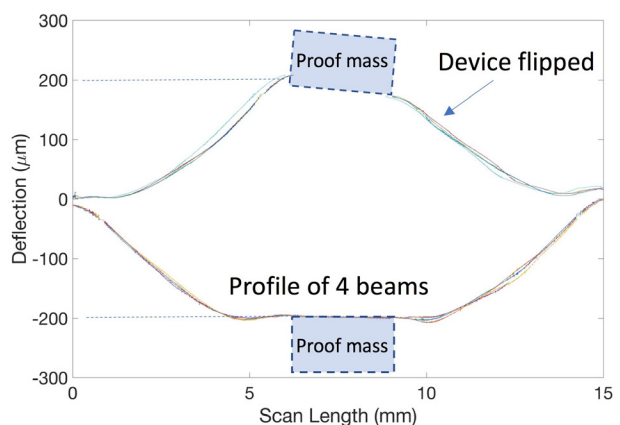
Vibration energy harvesters based on the resonance of the beam structure work effectively only when the operating frequency window of the beam resonance matches that of the available vibration source. None of the resonating micro-electro-mechanical system (MEMS) structures can operate with low-frequency, low-amplitude, and unpredictable ambient vibrations since the resonant frequency rises as the structure gets smaller. A bi-stable buckled beam energy harvester is has been developed to lower the operating frequency window below 100Hz for the first time at the MEMS scale. This design does not rely on the resonance of the MEMS structure but operates with the large snapping motion of the beam at very low frequencies when input energy overcomes an energy threshold. A fully functional piezoelectric MEMS energy harvester was

designed, monolithically fabricated, and tested.

An electromechanical lumped parameter model was developed to analyze the nonlinear dynamics and to guide the design of the nonlinear oscillator-based energy harvester. Multi-layer beam structure with residual stress-induced buckling was achieved through the progressive residual stress control of the deposition processes along with fabrication steps. The surface profile of the released device shows bi-stable buckling of  $200\mu\text{m}$ , which matches well with the amount of buckling designed. Dynamic testing demonstrates that the energy harvester operates with 50% bandwidth under 70Hz at 0.5g input, operating conditions that have not been demonstrated by MEMS vibration energy harvesters before.



▲ Figure 1: Photograph of released buckled beam energy harvesting device.



▲ Figure 2: Surface profile of four beams displaying buckling on both sides.

## FURTHER READING

- R. Xu, "Low-frequency, Low-Amplitude MEMS Vibration Energy Harvesting," Doctoral Thesis, Massachusetts Institute of Technology, Cambridge, 2018.
- R. Xu and S-G. Kim, "Modeling and Experimental Validation of Bi-stable Beam Based Piezoelectric Energy Harvester," *Energy Harvesting and Systems*, vol. 3, no. 4, pp. 313-21, Oct. 2016.
- A. Hajati and S-G. Kim, "Ultra-wide Bandwidth Piezoelectric Energy Harvesting," *Applied Physics Letts.*, vol. 99, no. 8, p. 083105, 2011.

# A Robust Electromagnetic MEMS Vibration Energy Harvester

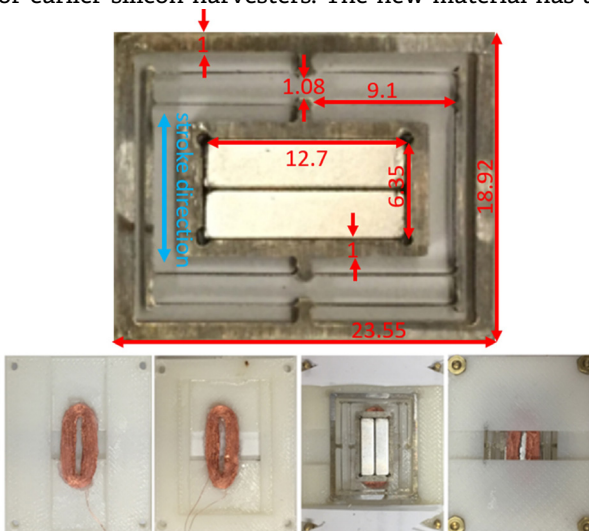
Y. Yang, U. Radhakrishna, J. F. Hunter, J. H. Lang  
Sponsorship: Analog Devices, Inc.

Modern production plants lack an effective way to autonomously monitor equipment health. It is uneconomical to engage personnel solely to monitor machines that function normally most of the time and impractical to wire plant-wide arrays of sensors for power and communication. As an alternative, vibration energy harvesters could power autonomous sensor networks that communicate wirelessly. Further, vibration-based machine health monitoring could be an effective method of assessing real-time machine performance. Such monitoring could become preventive by prompting maintenance prior to unrecoverable plant failures. To this end, this project seeks to advance the state of vibration energy harvesting.

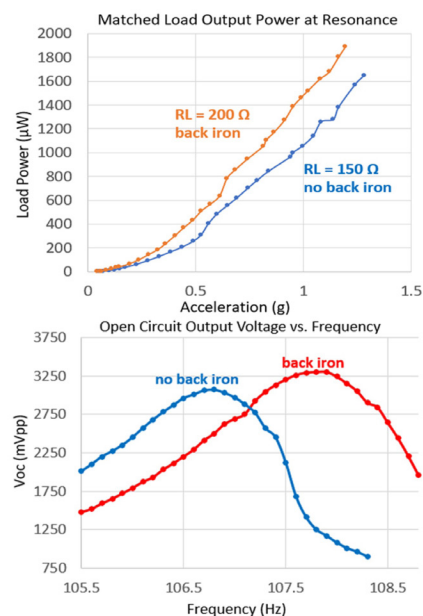
Our previous work yielded silicon-micro-electro-mechanical systems (MEMS) electromagnetic vibration energy harvesters suitable for powering machine health sensors. To further improve robustness and increase electrical power output, a new harvester is designed, fabricated, and demonstrated using the MP35N alloy. Its design and optimization follow that developed for earlier silicon harvesters. The new material has a

mechanical modulus close to that of the silicon while not being brittle. Thus, with similar material thickness, we maintain the harvester footprint while improving robustness. The MP35N alloy allows for less stressful full stroke operation, enabling improved output power while being much more tolerant of external shock.

Fabrication of the new harvester combines electric discharge machining and water-jet cutting for prototype production. The Lorentz-force harvester, with its folded-spring-suspended magnets, is packaged between two coupling coils using 3D-printed plastic package parts. The new harvester can survive large transient accelerations, common in an industrial setting; such accelerations are unsustainable by a comparable silicon harvester. This added durability brings the harvester much closer to practical application. The improved robustness enables the installation of back-irons, further improving the output power. The power output and power density (1.47 mW/cm<sup>3</sup>) are comparable to that of the previous record-setting silicon device.



▲ Figure 1: Top, MP35N harvester with dimensions labeled in mm. Bottom, left to right, the package parts with top and bottom coil, half-assembled harvester, and fully assembled one.



▲ Figure 2: Performance plots of the MP35N harvester. Note that data includes measurement results of harvester with and without addition of back irons.

## FURTHER READING

- A. Shin, U. Radhakrishna, Q. Zhang, L. Gu, P. Riehl, and A. P. Chandrakasan, J. H. Lang, "A MEMS Magnetic-based Vibration Energy Harvester," *2017 Power MEMS, J. of Physics: Conf. Series 1052*, p. 012082, 2018.
- U. Radhakrishna, P. Riehl, N. Desai, P. Nadeau, Y. Yang, A. Shin, J. H. Lang, and A. P. Chandrakasan, "A Low-power Integrated Power Converter for an Electromagnetic Vibration Energy Harvester with 150 mV-AC Cold Startup, Frequency Tuning, and 50 Hz AC-to-DC Conversion," *IEEE Custom Integrated Circuits Conference (CICC)*, 2018.

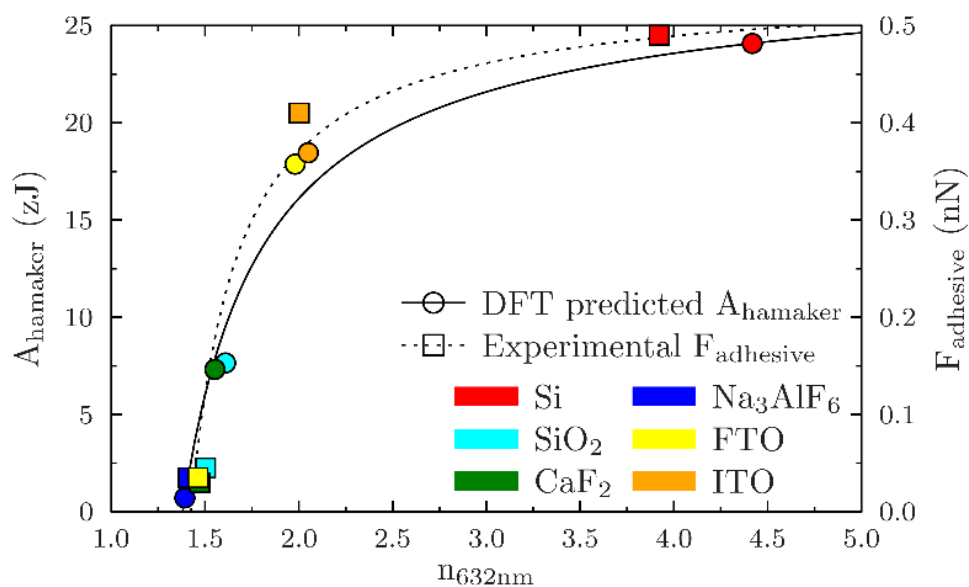
## Foulant-agnostic Coatings for Extreme Environments

C. Toparli, M. Carlson, M. A. Dinh, B. Yildiz, M. P. Short  
Sponsorship: Exelon

Fouling is ubiquitous in large-scale energy production, decreasing efficiency and increasing cost due to foulant buildup. Fouling degrades systems that rely on fluid flow and heat transfer by increasing system pressure drops, impeding heat transfer, and accelerating corrosion by fostering oxidation or concentrating chemical species within the foulant itself. This leads directly to system derating and early failure. To restore these functions, the deposits must be removed by techniques such as ultrasonic cleaning or manual removal, or the affected part must be replaced. However, these actions are often impractical, prolonging system outages and incurring significant costs due to downtime and component replacement. Therefore, it is crucial to prevent foulant deposition in the first place. The adhesion of foulant particles is due to their interaction with material surfaces, which can comprise many different types of surface forces. This attraction is dominated by van der Waals (vdW) forces in extreme environments of interest to large-scale energy production, where temperatures

and pressures are too high to support electrochemical double layers, and in the absence of other forces like magnetism, static charge, or steric bonding. Therefore, minimizing vdW forces should create an atomistically slick surface, preventing foulant deposition.

Here, we hypothesize and experimentally demonstrate a design principle for anti-fouling coatings that exploits the relation between vdW forces and the refractive index of the coating, when vdW forces are dominant. These coatings can be made foulant-agnostic. Both experimental results and first-principles calculations support our hypothesis. As can be seen in Figure 1, the findings show that the closer the refractive index spectrum of a coating to the surrounding fluid, the better it resists the deposition of all foulants. Immediate implications include improving the efficiency of both geothermal reservoirs and nuclear power plants, which are two of the largest sources of carbon-free electricity.



▲ Figure 1: Comparison of DFT calculated Hamaker constant, refractive index, and adhesive force obtained experimentally.

### FURTHER READING

- T. Allen, J. Busby, M. Meyer, and D. Petti, "Materials Challenges for Nuclear Systems," *Mater. Today*, vol. 13, no. 12, pp. 14–23, 2010.
- N. Mundhenk, et al., "Corrosion and Scaling as Interrelated Phenomena in an Operating Geothermal Power Plant," *Corr. Sci.*, vol. 70, pp. 17–28.
- J. N. Israelachvili, "6 - Van der Waals Forces in Intermolecular and Surface Forces," *Intermolecular and Surface Forces*, 3rd ed. San Diego, CA: Academic Press, pp. 107–132, 2011.

# All-solid-state Glucose Fuel Cell for Energy Harvesting in the Human Body

P. Simons, M. A. Gysel, J. L. M. Rupp

Efficiently powering sensors, pacemakers, and bio-electronic devices for the human body defines a new era of medicine to track, support, and operate bodily functions. Glucose fuel cells have seen a renaissance in recent years as an implantable power source harvesting energy from readily available fuels in the human body. Compared to existing implantable batteries, glucose fuel cells require much less frequent replacement surgery. However, state-of-the-art glucose fuel cells are based primarily on relatively bulky polymer electrolytes, suffer from long-term stability issues, and exhibit low power densities.

Here, we innovate a miniaturized glucose fuel cell that is fully composed of solid-state materials based on thin film processing. This all-solid-state glucose fuel cell can be scaled down to the sub-micrometer range for unprecedented miniaturization and is built on a Si chip using semiconductor fabrication methods suitable for integrated and direct powering

of bio-electronic implants. Through the use of abiotic catalysts instead of conventional biological catalysts such as enzymes and microbes, long-term stability and increased power density are in perspective. Free-standing fuel cell membranes based on a proton conducting oxide on Si chips were assembled using a microfabrication route with standard semiconductor processing techniques. Oxide thin films were prepared via pulsed laser deposition. The anode is in contact with glucose in phosphate-buffered saline solution to mimic blood, whereas the cathode is in contact with oxygen. Performance characterizations were carried out via electrochemical impedance spectroscopy and galvanostatic polarization curve measurements. We report that the proposed cell is electrochemically active and shows promise in functioning as the first all-solid-state glucose fuel cell with a roughly 100-fold lowered thickness of the device (only 250 nm) compared to polymer-based glucose fuel cells.

---

## FURTHER READING

- P. Simons and J. L.M. Rupp, *US Patent Application* US 15/901,732 (2018)
- Y. Shi, A.H. Bork, S. Schweiger, J.L.M. Rupp, *Nat. Mater.*, 14 (2015) 721-727.
- S. Kerzenmacher, J. Ducreé, R. Zengerle, F. von Stetten, *J. Power Sources*, 182 (2008) 1-17.